

Cross-correlation of WISE Galaxies with the Cosmic Microwave Background

Tomotsugu Goto¹, István Szapudi¹, Benjamin R. Granett²

¹*Institute for Astronomy, University of Hawaii 2680 Woodlawn Drive, Honolulu, HI, 96822, USA*

²*Istituto Nazionale di Astrofisica - Osservatorio Astronomico di Brera, Via E. Bianchi 46, 23807 Merate, Italy*

30 May 2018; in original form 2011 July 14

ABSTRACT

We estimated the cross-power spectra of a galaxy sample from the *Wide-field Infrared Survey Explorer* (WISE) survey with the 7-year *Wilkinson Microwave Anisotropy Probe* (WMAP) temperature anisotropy maps. A conservatively-selected galaxy sample covers $\sim 13000 \square^\circ$, with a median redshift of $z=0.15$. Cross-power spectra show correlations between the two data sets with no discernible dependence on the WMAP Q, V and W frequency bands. We interpret these results in terms of the the Integrated Sachs-Wolfe (ISW) effect: for the $|b| > 20^\circ$ sample at $\ell = 6-87$, we measure the amplitude (normalized to be 1 for vanilla Λ CDM expectation) of the signal to be 3.4 ± 1.1 , i.e., 3.1σ detection. We discuss other possibilities, but at face value, the detection of the linear ISW effect in a flat universe is caused by large scale decaying potentials, a sign of accelerated expansion driven by Dark Energy.

Key words: cosmology:early universe

1 INTRODUCTION

Dark Energy (DE) is the principal puzzle of twenty-first century physics. When identified with vacuum energy, the quantum field theory prediction for it is either 122 orders of magnitude too high or it is zero (Caldwell & Kamionkowski 2009). Both predictions glaringly contradict astronomical observations suggesting that the amount of DE today is of the same order of magnitude as that of Dark Matter. The existence of DE rests on measurements of the cosmic microwave background fluctuations (CMB), particularly by the *Wilkinson Microwave Anisotropy Probe* satellite (WMAP) constraining essentially the total energy density in the universe (Komatsu et al. 2011), and the low redshift acceleration of the universe detected, e.g., through supernovae (Riess et al. 1998). The evidence for DE appears to be overwhelming today, albeit indirect. Most present and future observations rely on standard candles and/or rulers to quantify the geometry and expansion history, or growth history of the universe (with the possible exception of gravitational lensing).

The Integrated Sachs-Wolfe (ISW Sachs & Wolfe 1967; Rees & Sciama 1968) effect promises a unique avenue to directly detect the effect of DE on CMB photons: as photons cross potential wells, they suffer both blue and redshift cancelling each other in a flat, DE-free universe where the potential wells are frozen. However, when DE is present, potential wells decay during the photon crossing, therefore the redshift fails to fully compensate for the blueshift. The net result is a slight “kick” the photon receives. This will ultimately result in a tiny correlation of hot spots in the CMB with large-scale structure, an effect which is orders of magni-

tude smaller than the CMB correlations (Crittenden & Turok 1996; Peiris & Spergel 2000).

Such correlations were measured in the literature between the WMAP and the Sloan Digital Sky Survey (SDSS) Luminous Red Galaxies (Scranton et al. 2003; Fosalba et al. 2003; Padmanabhan et al. 2005; Granett et al. 2008; Pápai et al. 2011), APM galaxies (Fosalba & Gaztañaga 2004), infrared galaxies (Afshordi et al. 2004), radio galaxies (Nolta et al. 2004; Raccanelli et al. 2008), and the hard X-ray background (Boughn & Crittenden 2004b,a). In addition to the ISW effect, CMB photons become correlated with the LSS at high ℓ (small scales) due to the Sunyaev-Zeldovich effect, and lensing. The latter was recently detected by Smith et al. (2007).

This analysis uses the first data release of the *Wide-field Infrared Survey Explorer* (WISE; Wright et al. 2010). We use a sample of galaxies over a survey area of $\sim 13000 \square^\circ$ with a median redshift of $z=0.15$. The combination of area and volume at moderate redshift has the potential to detect (or reject) the ISW effect more clearly than previous studies.

2 ANALYSIS AND RESULTS

2.1 Data

For the CMB, we use the WMAP 7-year data set (Komatsu et al. 2011). We use the Q, V and W foreground removed maps. We rebin the maps in Healpix format to $n_{\text{side}} = 128$ for a pixel size of $27'/\text{pixel}$ (Górski et al. 2005). We apply the Temperature Analysis Mask provided by the WMAP team to exclude regions of Galactic emission and known point sources leaving about 78% of sky.

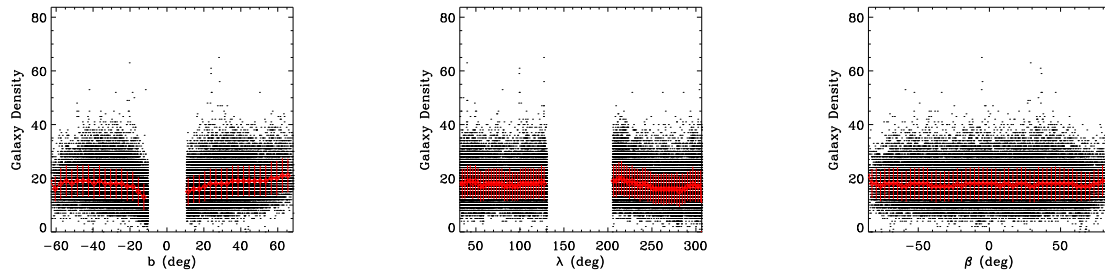


Figure 2. Galaxy number density (in $27'$ pixels) as a function of Galactic latitude b and ecliptic coordinates β and λ . The red line connects median values, with RMS in the red vertical lines.

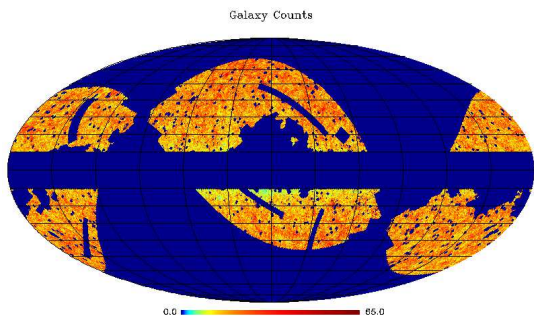


Figure 1. Galaxy counts from the WISE galaxy sample. Regions with zero galaxy counts are masked out by the object masks used for the WISE galaxy and WMAP sample. These are regions with $|b| < 10$ deg, missing data, and star clusters.

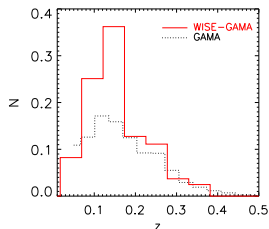


Figure 3. The normalized redshift distributions of the WISE galaxy sample (red solid line) and the GAMA spectroscopic sample (black dotted line).

The WISE satellite surveys the entire sky at wavelengths of 3.4, 4.6, 12, and $22 \mu\text{m}$ ($W1$ through $W4$), with the point source sensitivities of 0.08, 0.11, 1, and 6 mJy, respectively. We use the first data release issued on April 14, 2011, containing about half the sky.

We need to remove stars from the WISE object catalogue. We find that most stars ($|b| < 10^\circ$) have a $3.4 - 4.6 \mu\text{m}$ color less than 0.2. Therefore, we apply a color cut of $3.4 - 4.6 \mu\text{m} > 0.2$ to select galaxies. We further apply a color selection of $4.6 - 12 \mu\text{m} > 2.9$, which removes a greater number of stars at the expense of a small number of galaxies. Due to the sun-synchronous orbit of the satellite, WISE data are deeper in pole regions. To select a uniform galaxy sample, we only use galaxies with $W1_{3.6 \mu\text{m}} < 15.2$ mag.

We construct Healpix maps of the galaxy counts matching our CMB maps, shown on Fig. 1. We apply the WMAP mask and additionally mask out regions with missing data and unusually

high object-counts such as star clusters and the Magellanic clouds. These can be seen as thin stripes in Fig. 1, totaling $613 \square^\circ$ of area. We also mask cells with more than 10 flagged sources (as persistent, halo, ghost, or spike). This helps to exclude cells contaminated by bright nearby galaxies and stars, as visual inspection of pixels in the tail confirmed. We do not use regions with $|b| < 10^\circ$ due to strong stellar contamination. Our galaxy catalog contains 1.2 million galaxies over an area of $13622 \square^\circ$ and the median galaxy density is 86 deg^{-2} .

We investigate gradients in the galaxy density in Fig. 2 as a function of Galactic latitude b , and ecliptic coordinates β and λ . There appears to be a significant decrease in the galaxy number density at $10 < |b| < 15$, reaching 30% at $|b| = 10^\circ$. At this low galactic latitude, Milky Way stars can mask background galaxies and confuse photometry. This effect has been studied in optical bands (Ross et al. 2011), but it is more severe in WISE due to the broader point spread function. In the middle panel, the galactic centre is at $\lambda \sim 270^\circ$, and the same effect can be seen. To test how this might affect our results, we analyse maps with three different galactic cuts ($|b| > 20^\circ$, 15° and 10°) in Section 2.3. The WISE data become deeper toward the pole regions, but there is no significant change in galaxy density as a function of β (right panel).

To estimate the expected ISW signal, we need to know the redshift distribution of our galaxy sample, and the galaxy bias. We have cross-matched the WISE galaxy sample with GAMA (Galaxy and Mass Assembly; Driver et al. 2011) sample to estimate a preliminary redshift distribution. GAMA is a spectroscopic sample of 205,000 galaxies observed with AAΩ 4m telescope. The survey depth is as deep as $r_{AB} < 20.5$ mag, and thus, deep enough to estimate the redshift distribution of the WISE galaxy sample. In the overlapping regions, 83% of the WISE galaxy sample had spectroscopic counterpart in GAMA. Fig. 3 shows the redshift distribution of the WISE galaxy sample with GAMA counterparts. The dotted black histogram shows the redshift distribution of the GAMA sample, which has a much longer tail toward higher redshift. The median redshift of the WISE-GAMA sample is $z=0.148$.

2.2 Galaxy bias

In order to determine galaxy bias, we measure the galaxy-galaxy angular power spectrum. The form of the angular power spectrum can be theoretically computed given cosmological parameters. We use the WMAP 7-year ΛCDM cosmological parameters ($H_0 = 70.4 \text{ km/s/Mpc}$, $\Omega_m = 0.272$). However, in linear theory, bias cannot be determined independently of σ_8 , the power spectrum is normalized as $C_l \propto (b\sigma_8)^2$, where b relates galaxy and matter overdensities as $\delta_g = b\delta_m$. We therefore use a fixed value

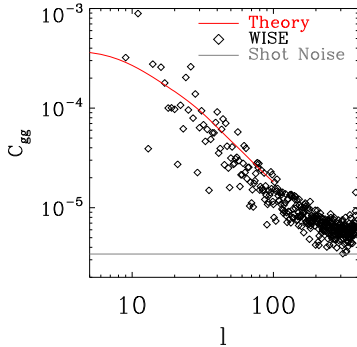


Figure 4. Auto correlation of the WISE galaxy sample ($|b| > 20^\circ$). The red solid curve is a fit of a theoretical matter power spectrum from CAMB with the latest cosmological parameters for Λ CDM. The gray solid line is a Poisson shot noise.

of $\sigma_8=0.80$, and fit the galaxy-galaxy angular correlation only for bias. We use CAMB with Halofit (Lewis et al. 2000; Smith et al. 2003) to generate non-linear matter powerspectra for our cosmological model, and obtain three-dimensional spectra at the median redshift of $z=0.148$. The angular power spectrum is a projection of the three-dimensional power spectrum with a kernel that depends on the redshift distribution:

$$C_l^{gg} = b_g^2 \frac{2}{\pi} \int \left[\int r^2 \phi(r) j_l(kr) dr \right]^2 k^2 P(k) dk, \quad (1)$$

with $\phi(r) \propto \frac{dN(r)}{dz} \frac{dz}{dV}$ for comoving coordinate r normalized such that $\int \phi(r) r^2 dr = 1$ and j_l is the spherical Bessel function. We make use of the small-angle limit with the Limber equation to evaluate the power spectrum at $l > 20$, see *e.g.*, Afshordi et al. (2004).

We compute the galaxy-galaxy angular power spectrum of the WISE galaxy sample using SpICE (Spatially Inhomogeneous Correlator Estimator; Szapudi et al. 2001a,b), a fast quadratic estimator which inverts the coupling matrix of the C_l 's in pixel space where it is diagonal. The resulting power spectrum of the WISE galaxy sample is shown in Fig. 4. The Poisson shot noise is given by $1/N$, where N is the mean number of galaxies per steradian. In our sample, $1/N = 3.4 \times 10^{-6}$, which is much smaller than the correlation at $l = 2 - 100$. We subtract the Poisson noise (gray line), then fit the amplitude of the model template over the range $l = 2 - 100$. We find a bias parameter of $b_g \equiv b\sigma_8/0.8 = 1.06 \pm 0.05$.

2.3 WISE-WMAP Cross Power Spectrum

We cross-correlate the WISE galaxy sample with the foreground-removed Q, V, and W maps from WMAP. Because of the declining galaxy density at low galactic latitude b (Fig.2), we show results in three different samples, $|b| > 10$, $|b| > 15$ and $|b| > 20$. But first, we show results with the $|b| > 20$ sample. The resulting angular power spectra are shown in Fig. 5. The spectrum (black dots) band powers are binned 0.15 dex logarithmic bins. The boundaries are $l=6,8,11,16,22,31,44,61$ and 87 such that the first band includes $l = 6,7$, etc. We do not use data at $l \geq 87$ since these small scales should not be sensitive to the ISW effect.

In order to estimate uncertainty in the WISE-WMAP cross power spectrum, we have run 1000 simulations. Using `synfast` and the latest Λ CDM cosmological parameters, we create 1000 random CMB maps. Cross-correlating these random CMB maps with

the WISE galaxy catalog, we estimated the covariance matrix. It is dominated by diagonal terms, i.e. neighboring band powers are uncorrelated to a good approximation.

The error bars plotted in Fig. 5 are given by the diagonal elements of the covariance matrix. The large-scale modes at $l < 6$ are not well constrained on the cut sky. The size of a contiguous survey region in the WISE map (Fig. 1) is $\sim 60^\circ$, or 30° in radius. This corresponds to a limiting scale of $l \sim 180^\circ/\theta \sim 6$. Therefore, we do not have strong constrains at $l < 6$. For simplicity we exclude the large-scale modes at $l < 6$ in the analysis.

The C_l 's are consistent among different WMAP frequencies, while most foregrounds from Milky Way emission should exhibit some color dependence.

Theoretical expectation for the ISW power spectrum from the the latest cosmological parameters for Λ CDM are plotted with the red solid line. We adopted bias the parameter of $b_g = 1.06$ estimated from auto-correlation in Section 2.2. The galaxy density-CMB cross power spectrum is given by (Cooray 2002),

$$C_l^{gT} = T_{CMB} \frac{3\Omega_m H_0^2}{c^2} b_g \frac{2}{\pi} \int k^2 dk P_k \times \int k^{-2} \frac{d(1+z)D_1(z)}{dr} j_l(kr) dr \int r'^2 \phi(r') j_l(kr') dr' \quad (2)$$

where $D_1(z)$ is the linear growth factor.

The measured power spectrum is higher than the Λ CDM prediction. To quantify this we scale the model with a free amplitude parameter. In Fig. 5, the best χ^2 -fit was in the orange line, which is 2.2σ larger than the original theoretical expectation.

2.4 Significance tests

We now test the following three hypotheses for consistency with the data: (a) theoretical best-fit ISW (orange line in Fig. 5), (b) theoretical ISW from vanilla Λ CDM (red line) (c) Null hypothesis: no power, i.e. no ISW effect.

We follow Francis & Peacock (2010) and compute χ^2 values using the covariance matrix for the three hypotheses. In Fig. 5, we see a high power at $l=9$ and 12, that drops at $l = 7$. The significances of correlation at $l = 9$ and 12 are 1.3 and 1.7σ , respectively. While the significance of an individual band power is affected by the binning, the final χ^2 values and likelihoods are robust. To check for this, tested alternative band powers with boundaries at $l=6,9,12,17,24,48,67$ and 95 (purple squares in Fig.5); none of our numerical results or conclusions changed.

The χ^2 statistic is given by $\chi^2 = (\mathbf{x} - \mathbf{t}_i)^T \mathbf{C}^{-1} (\mathbf{x} - \mathbf{t}_i)$ for the observed data vector \mathbf{x} and a given theoretical expectation \mathbf{t}_i for model i . For $l=6-87$ with 8 data points, the χ^2 values are 11.6, 16.1 and 20.7 for (a), (b), and (c), respectively. The χ^2 values decrease significantly for the ISW models (a) and (b) compared with the null hypothesis. Computed $\Delta\chi^2$ (Ratio of evidence) are 9.2 for $l=6-87$. Generally, $\Delta\chi^2 \geq 3$ can be considered as strong evidence. Our best-fit measurement has $\Delta\chi^2 > 3$ in all cases.

In terms of the likelihood ratio, $e^{1/2\Delta\chi^2}$, we obtain 97 and 9.9 as shown in Table1. The likelihood ratio is considered significant if it is greater than 5. According to these ratios of evidence, the ISW hypotheses (a) and (b) are preferred over the null hypothesis.

For the model (a), these numbers can be compared with the significance of the amplitude fit itself. We computed $1-\sigma$ errors of the fit of the theoretical ISW model to the data, by estimating the 68 percentile of the $e^{-1/2\chi^2}$ distribution. We also checked that the measured errors are consistent with the width of the best-fit Gaus-

sian. Results in Table 2 show that the best-fit model is 3.1σ from the null hypothesis.

2.5 Systematic tests

We have shown results with $|b| > 20^\circ$ sample. In this section, we explore if changing the galactic cut affects our results.

With a $|b| > 15^\circ$ cut, we have $\sim 1700 \square^\circ$ more area than the $|b| > 20^\circ$ cut. The resulting amplitude of the best-fit ISW model is 3.2 ± 1.1 , i.e., 2.9σ , in agreement with the result from $|b| > 20^\circ$. As shown in Table 1, the $\Delta\chi^2$ and likelihood ratio are decreased, but are not significantly changed. At $|b| \sim 15^\circ$ the galaxy density starts to decline towards the galactic plane, and thus, the correlation signals have been reduced some, but overall, we obtained consistent results with the $|b| > 20^\circ$ analysis.

Next we used $|b| > 10^\circ$ sample. This sample adds another $\sim 1600 \square^\circ$. As shown in Tables 1 and 2, the signal becomes lower and the error is larger giving a worse significance of 2.0σ . This is most-likely due to the systematic decrease in galaxy density at low b , where artefacts of bright stars and high stellar density decrease the galaxy density. Large-scale gradients in the galaxy distribution can increase the measurement errors because they are amplified by cosmic variance of the CMB on large angular scales.

To test this interpretation, we artificially flattened the galaxy density as a function of b , by dividing the galaxy density by the mean galaxy density at each b . This process can be considered as a high pass filtering that removes large-scale gradients. As shown in Tables 1 and 2, the significance is increased to 3.2σ , becoming consistent with values we measured with $|b| > 20^\circ$ and 15° samples.

To the opposite direction, we tried $|b| > 25^\circ$, again obtaining a consistent amplitude of 3.5 ± 1.2 (Tables 1 and 2). These tests show that our results are robust, obtaining $\sim 3 \sigma$ significance regardless the choice in the galactic cut b .

We briefly discuss stellar contamination next. Stars are not clustered, but star counts might be correlated with the CMB due to galactic contamination. According to Fig. 2, the galaxy density is constant at $|b| > 20$, although there is a slight negative gradient at $|b| < 20$. We argue that is likely to be due to artefacts and confusion with stars. The robustness of the results with respect to galactic cuts, however, implies that the effect on the correlations is negligible for the foreground subtracted CMB maps we use. We do not see any significant colour dependence either between WMAP frequencies (V , W , and Q) in Fig. 5. These points suggest that the stellar contamination is small, or at least uniform across our survey area. In the worst case the contamination would be 17%, if all unidentified GAMA sources were stars, but it is likely to be much less.

3 DISCUSSION AND CONCLUSIONS

The significant correlations between WMAP and WISE on large scales may have contributions from many sources including the Milky Way, extragalactic point sources, even zodiacal light. We have attempted to minimize contamination by constructing a clean galaxy sample from WISE. We find no systematic trends in galaxy number density with ecliptic latitude and longitude (Fig. 2). We use the WMAP foreground reduced CMB maps to reduce the sensitivity to Milky Way emission in WMAP bands. The primary sources (dust, synchrotron and free-free emission) have characteristic spectral shapes across the WMAP frequency bands. The ex-

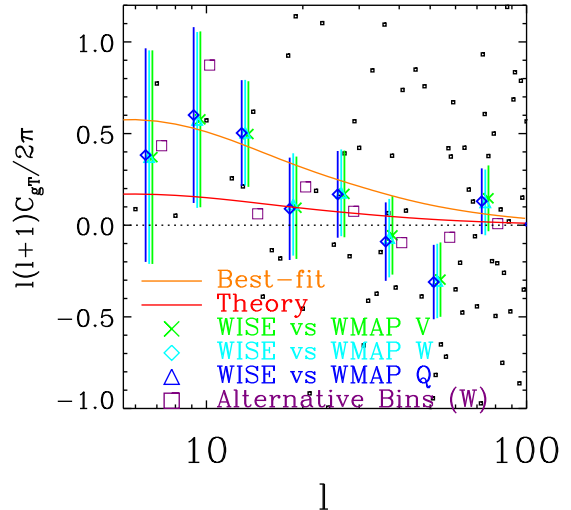


Figure 5. Power spectra between the WISE galaxy sample ($|b| > 20^\circ$) and WMAP (V,Q,W) maps. The data in original resolution (black dots) are binned in 0.15 dex logarithmic bins and shown with error bars. The red solid line is theoretical expectation with the bias of 1.06, while the orange line is the best fit to the observed data. The fit used 8 ($l=6-87$) data points. The purple line is from WMAP W data in different binning.

Table 1. Significances from χ^2 tests at $l = 6 - 87$.

Galactic cut		χ^2	d.o.f.	$\Delta\chi^2$	Likelihood ratio
$ b > 25^\circ$	Best-fit ISW	10.2	7	8.7	77
	ISW with Λ CDM	14.7	8	4.2	8.2
	Null hypothesis	18.9	8	0	-
$ b > 20^\circ$	Best-fit ISW	11.6	7	9.2	97
	ISW with Λ CDM	16.1	8	4.6	9.9
	Null hypothesis	20.7	8	0	-
$ b > 15^\circ$	Best-fit ISW	11.0	7	8.1	59
	ISW with Λ CDM	14.9	8	4.3	8.6
	Null hypothesis	19.2	8	0	-
$ b > 10^\circ$	Best-fit ISW	9.1	7	3.8	6.6
	ISW with Λ CDM	11.1	8	2.6	3.2
	Null hypothesis	13.7	8	0	-
$ b > 10^\circ$ with flattening	Best-fit ISW	14.3	7	10.2	166
	ISW with Λ CDM	19.1	8	5.4	14.8
	Null hypothesis	24.5	8	0	-

Table 2. Amplitude and errors of the best-fit ISW model at $l=6-87$.

Sample	Area (\square°)	Amplitude and error	σ
$ b > 25^\circ$	8495	3.5 ± 1.2	3.1
$ b > 20^\circ$	10337	3.4 ± 1.1	3.1
$ b > 15^\circ$	12032	3.2 ± 1.1	2.9
$ b > 10^\circ$	13622	2.6 ± 1.3	2.0
$ b > 10^\circ$ with flattening	13622	3.2 ± 1.0	3.2

cellent agreement between the Q, V and W spectra (Fig. 5) leads us to believe that Galactic foregrounds are unimportant.

Extragalactic point sources below the WMAP detection limit could also contaminate the signal. Since WISE is a near-IR survey, galaxies detected in WISE may also emit strongly at WMAP frequencies. Such sources would produce a characteristic signal in the power spectrum that could become important on small scales. The zeroth order estimate of this effect is a Poisson term with a flat C_l spectrum; no evidence for this is seen at $l < 87$. Similarly, the Sunyaev-Zeldovich effect is expected to appear at higher l and has negligible effect at $l < 87$ (Fosalba & Gaztañaga 2004; Afshordi et al. 2004).

We leave detailed discussion of the cosmological significance to a future work, a few comments will suffice here. Our best fit ISW model is 2.2σ higher than Λ CDM expectation. This is consistent with many previous cross-correlation measurements (Ho et al. 2008; Giannantonio et al. 2008; Granett et al. 2009) that had higher amplitude than vanilla Λ CDM prediction. Possible reasons include uncertainties in cosmological parameters or our galaxy bias model. Additionally, the measurement is subject to significant cosmic variance originating from both the CMB and LSS fields (Pápai et al. 2011). At present there is at most a mild tension between vanilla Λ CDM and measurements that is not fully understood.

In the Λ CDM model, the amplitude of the ISW signal is well constrained by our knowledge of σ_8 , the Hubble constant and the matter density. However, we do face uncertainty in the redshift distribution and its effect on our estimate of the linear bias and the amplitude of the ISW spectrum. We obtained the dN/dz by matching the WISE galaxy sample to the GAMA spectroscopic sample. Although the GAMA sample is deep, it is an optically selected sample while WISE is sensitive to the near IR. Thus, GAMA may be missing a population of WISE galaxies such as heavily obscured one. We checked the fraction of our WISE galaxy sample detected by GAMA was 83%. While 83% is a large fraction, the redshift distribution of the rest 17% is unknown.

However, even if we assume this 17% of galaxies are all at higher redshift than 0.148, the median only changes to $z=0.155$. More generally, to test whether erroneous redshift distribution can affect bias estimate, we have artificially shifted the median redshift from $z=0.09$ to $z=0.22$, a value clearly beyond reasonable. The change in bias is within 40%. Therefore, the errors in the redshift estimation alone can only account for a fraction of the shift between the original and best-fit theoretical ISW estimations. Furthermore, the amplitude of the ISW spectrum is relatively insensitive to the median redshift over this range.

The most relevant measurements in the literature to compare with are from 2MASS for which weak and null detections of the ISW signal have been claimed (Rassat et al. 2007; Francis & Peacock 2010). However, the median redshift of 2MASS is $z=0.07$ and in terms of comoving volume, the WISE sample is 4.6 times larger. Francis & Peacock (2010) selected a higher redshift sample ($0.2 < z < 0.3$) using photometric redshifts but it is also much more sparse. The WISE sample may be situated in an ISW ‘sweet spot’: it is a large volume and samples a low redshift when dark energy has come to dominate the cosmic expansion. Indeed, the WISE survey seems in better agreement with higher redshift datasets (Ho et al. 2008; Giannantonio et al. 2008). However, the Λ CDM expectations are at the detection limit for current surveys. It is possible that we are only measuring the ISW signal from “lucky” statistical fluctuations that push the signal above the typical $2\text{-}\sigma$ detection threshold leading to biased conclusions if taken at face value. Future surveys that expand on the sky coverage and

redshift range in the next decade will provide a clearer picture on the integrated Sachs-Wolfe effect and the role of dark energy.

We thank the anonymous referee for many insightful comments. We acknowledge financial support from the NASA grant NNX10AD53G and the Polanyi program of the Hungarian National Office for the Research and Technology (NKTH).

REFERENCES

- Afshordi N., Loh Y.-S., Strauss M. A., 2004, *Phys. Rev. D.*, 69, 8, 083524
- Boughn S., Crittenden R., 2004a, *Nature*, 427, 45
- Boughn S. P., Crittenden R. G., 2004b, *ApJ*, 612, 647
- Caldwell R. R., Kamionkowski M., 2009, *Annual Review of Nuclear and Particle Science*, 59, 397
- Cooray A., 2002, *Phys. Rev.*, D65, 103510
- Crittenden R. G., Turok N., 1996, *Physical Review Letters*, 76, 575
- Driver S. P., Hill D. T., Kelvin L. S., et al., 2011, *MNRAS*, 413, 971
- Fosalba P., Gaztañaga E., 2004, *MNRAS*, 350, L37
- Fosalba P., Gaztañaga E., Castander F. J., 2003, *ApJL*, 597, L89
- Fosalba P., Gaztañaga E., 2004, *MNRAS*, 350, L37
- Francis C. L., Peacock J. A., 2010, *MNRAS*, 406, 2
- Giannantonio T., Scranton R., Crittenden R. G., et al., 2008, *Phys. Rev. D.*, 77, 12, 123520
- Górski K. M., Hivon E., Banday A. J., et al., 2005, *ApJ*, 622, 759
- Granett B. R., Neyrinck M. C., Szapudi I., 2008, *ApJL*, 683, L99
- Granett B. R., Neyrinck M. C., Szapudi I., 2009, *ApJ*, 701, 414
- Ho S., Hirata C., Padmanabhan N., Seljak U., Bahcall N., 2008, *Phys. Rev. D.*, 78, 4, 043519
- Komatsu E., Smith K. M., Dunkley J., et al., 2011, *ApJS*, 192, 18
- Lewis A., Challinor A., Lasenby A., 2000, *ApJ*, 538, 473
- Nolta M. R., Wright E. L., Page L., et al., 2004, *ApJ*, 608, 10
- Padmanabhan N., Hirata C. M., Seljak U., Schlegel D. J., Brinkmann J., Schneider D. P., 2005, *Phys. Rev. D.*, 72, 4, 043525
- Pápai P., Szapudi I., Granett B. R., 2011, *ApJ*, 732, 27
- Peiris H. V., Spergel D. N., 2000, *ApJ*, 540, 605
- Raccanelli A., Bonaldi A., Negrello M., Matarrese S., Tormen G., de Zotti G., 2008, *MNRAS*, 386, 2161
- Rassat A., Land K., Lahav O., Abdalla F. B., 2007, *MNRAS*, 377, 1085
- Rees M. J., Sciama D. W., 1968, *Nature*, 217, 511
- Riess A. G., Filippenko A. V., Challis P., et al., 1998, *AJ*, 116, 1009
- Ross A. J., Ho S., Cuesta A. J., et al., 2011, *MNRAS*, 417, 1350
- Sachs R. K., Wolfe A. M., 1967, *ApJ*, 147, 73
- Scranton R., Connolly A. J., Nichol R. C., et al., 2003, *astro-ph/0307335*
- Smith K. M., Zahn O., Dore O., 2007, *ArXiv e-prints*, 705
- Smith R. E., Peacock J. A., Jenkins A., et al., 2003, *MNRAS*, 341, 1311
- Szapudi I., Prunet S., Colombi S., 2001a, *ApJL*, 561, L11
- Szapudi I., Prunet S., Pogosyan D., Szalay A. S., Bond J. R., 2001b, *ApJL*, 548, L115
- Wright E. L., Eisenhardt P. R. M., Mainzer A. K., et al., 2010, *AJ*, 140, 1868